Contents lists available at ScienceDirect

Journal of Molecular Liquids

journal homepage: www.elsevier.com/locate/molliq



Examining the structure and intermolecular forces of thiazolium-based ionic liquids



Christine Castillo ^a, Erica Chenard ^a, Matthias Zeller ^b, Nahla Hatab ^c, Pasquale F. Fulvio ^{d,*}, Patrick C. Hillesheim ^{a,*}

- ^a Department of Chemistry and Physics, Ave Maria University, 5050 Ave Maria Blvd, Ave Maria, FL 34142, USA
- ^b Department of Chemistry, Purdue University, 560 Oval Drive, West Lafayette, IN 47907-2084, USA
- ^c Department of Chemistry, University of Tennessee, 1621 Cumberland Ave, Knoxville, TN, 37996, Knoxville, USA
- ^d Department of Nuclear Engineering, Texas A&M University, College Station, TX 77843, USA

ARTICLE INFO

Article history: Received 23 September 2020 Received in revised form 8 November 2020 Accepted 13 November 2020 Available online 18 November 2020

Keywords:
Ionic liquids
Hirshfeld surfaces
Crystal structure
Thermal analysis
Physicochemical properties
Intermolecular forces

ABSTRACT

A series of seven novel thiazolium-based ionic liquids have been synthesized and characterized. To understand the physicochemical properties of thiazolium ionic liquids the compounds were characterized via thermogravimetric analysis, differential scanning calorimetry, and powder X-ray diffraction. The thiazolium sulfur atom is found to impart unique intermolecular interactions affecting the properties of the materials, both in the solid and liquid state. These interactions are examined by Hirshfeld surface analysis of single-crystal X-ray diffraction data as well as via variable-temperature viscometry. Further, it was observed that several of the ionic compounds exhibit high enthalpies of fusion making them potential candidates for thermal energy storage materials, expanding the possible applications for this class of compounds.

© 2020 Elsevier B.V. All rights reserved.

1. Introduction

Ionic liquids (ILs) are a class of semi-organic compounds which are broadly classified as an organic cation-inorganic anion pair which melt below 100 °C [1]. ILs have been applied in a wide breadth of fields such as catalysis [2], non-aqueous electrolytes [3,4], alternative materials for carbon capture [5], as solvents for biomass processing [6,7], as well as a host of other applications. There is an increasing demand for sustainable sources of energy, especially for energy storage and conversion materials. However, all renewable energy sources have the disadvantage of intermittent supply and lack of storage media [8]. ILs have generated interest for thermal energy storage at temperatures in the 75–200 °C range which is not easily achieved with traditional materials [9,10]. Traditional phase change materials (PCMs) have a low thermal storage density, undergo significant transitions during phase changes, and can suffer from issues caused by supercooling as well as being potentially corrosive [8]. Given their ionic nature, ILs have the potential to transfer thermal energy in the latent heat of a phase transitions, and ILs with high enthalpies of fusion can transfer significant amounts of energy to their immediate surroundings during their phase transitions. One of the desirable features of ILs in thermal energy storage is their expanded liquidus range [9,11]. The melting point and the enthalpy of fusion can be tailored by careful choice of the structure of the cation and anion [12]. For example, Zhu et al. have reported that long-chain ILs, such as 1-hexadecyl-3-methylimidazolium bromide, or [C_{16} -Mim][Br], exhibit favorable thermophysical properties values suitable for use as PCMs [13]. This work was followed by Bendová et al. in which they examined ionic liquid compounds [C_{16} -Mim] with differing anions, namely chloride and saccharinate [14]. The long-chain alkyl imidazolium ILs displayed melting points of ~51 °C and 65 °C and it was concluded that the structure of the anion affects the enthalpies of fusion and the heat capacity.

One key feature of ILs which allows for their wide-spread application comes from the high potential for synthetic customization of both the cation and anion. Thus, it follows that the structure of ILs has a significant impact on the properties of the formed cationanion pair. As an example, the most studied IL systems consist of heterocyclic cations, such as an imidazolium, often paired with fluorinated anions, such as hexafluorophosphate $[PF_6^{1-}]$, tetrafluoroborate $[BF_4^{1-}]$, or bis(trifluoromethane)sulfonimide $[Tf_2N^{-}]$ [15–17]. In these imidazolium-based compounds, the fluorinated anions impart favorable properties like low viscosity, increased hydrophobicity,

^{*} Corresponding authors. *E-mail addresses*: pfulvio@tamu.edu (P.F. Fulvio), Patrick.Hillesheim@avemaria.edu (P.C. Hillesheim).

and high thermal stability [1,18,19]. The halide-based ILs of the same imidazolium compounds, however, tend to exhibit higher melting points, increased crystallinity, and significantly lower material costs [1,3,15,16].

Alkyl chain length is another variable synthetic point for ILs. Varying alkyl chain length has been demonstrated to affect a number of properties including thermal stability [20,21], onsets of phase transitions [18], and gas solubilities [1,22]. For example, examining the properties of imidazolium based ILs with the [Tf₂N⁻] anions bearing alkyl chain lengths from 2 carbons (ethyl) to 6 carbons (hexyl) to 16 carbons (hexadecyl) show an increase in melting point from approximately $-17 \,^{\circ}\text{C}^{19}$ to $-7 \,^{\circ}\text{C}^{23}$ to 42 $^{\circ}\text{C}$ [24], respectively. However, increases in alkyl chain length also affects the density with the general trend being that increases in alkyl chain length decrease the density of the formed IL [25]. It should be noted, however, that these properties, among others, are merely discussed herein as trends. The overall properties of any set of ILs is dependent on many factors, of which alkyl chain length, cation structure, heteroatom presence, or anion structure comprise just a portion of the potential tailorable points affecting the final properties [1,17,18].

For instance, the structure property relationship of several related heterocyclic ILs having the 1,2,3-triazolium [26], 1,2,4-triazolium [27], and pyridinium [28] based ILs have been reported. When compared with their imidazolium congeners, and given the complex nature of ILs, the properties of the various triazolium and pyridinium based compounds exhibit a wide range of potentially favorable attributes. For instance, the 1,2,3-triazolium based ILs exhibit increased stability under basic conditions due to the lack of a hydrogen at the C2 position on the ring [26]. Pyridium based salts have been shown to form liquid crystalline materials based on variations in the alkyl chain length [29]. The pyridinium ILs also exhibited comparable thermal properties to their imidazolium counterparts, allowing for their potential use as alternative materials [23].

Compared to imidazolium, pyridinum, and triazolium ILs, another class of less investigated compounds is that of ILs based on the thiazole heterocyclic ring. The thiazole ring has one N and one S atom in the same five-membered ring, and the combination of two distinct heteroatoms yield unique properties to the resulting ILs. For example, thiazolium based ILs have desirable properties for gas separations [30], lubricants [31], and even as catalysts for heterocycle synthesis [32]. Encouragingly, it has been recently demonstrated that incorporation of sulfur moieties into ionic liquid cations has imparted unique properties such as lowering the melting point [33] as well as providing modular platforms for synthesis of task-specific ionic liquids [34]. These recent advances further show the importance of fundamental studies into novel cationic moieties leading to ILs.

To date, limited reporting in the literature with respect to their synthesis, physicochemical, and structural evaluation of thiazolium based ILs makes these compounds even more attractive from a synthetic view point. Herein we report the synthesis and characterization of seven novel thiazolium-based ionic liquids with the [Tf₂N⁻] anion. The alkyl side chain of the cation was varied from C_2 to C_{16} . The physicochemical properties of the thiazolium ILs were examined using thermogravimetric analysis (TGA), dynamic scanning calorimetry (DSC), and viscometry. While the viscosity systematically increased with increasing alkyl chain length, the density and decomposition temperature decreased in the same order. Further, crystal structures of both the butyl thiazolium bromide and tetradecyl thiazolium [Tf₂N⁻] derivatives were examined via singlecrystal and powder X-ray diffraction. Six of the compounds can be classified as classical ionic liquids with melting points below 100 °C, with four of the compounds existing as free-flowing liquids near or below room temperature. Further, three of the compounds exhibit phase transitions with high enthalpies making them potential candidates for thermal energy storage materials.

2. Materials and methods

2.1. Chemicals

Thiazole and lithium bis(trifluoromethane)sulfonimide were purchased from ChemImpex. Bromoethane, 1-bromobutane, 1-bromohexane, and 1-bromooctane, 1-bromodoceane, 1-bromohexadecane and solvents were purchased from Fisher Scientific. All chemicals were purchased in the highest purity available. Synthesized ionic liquid compounds were labeled according to the substituting linear alkyl chain length in the thiazolium cation as C_n -Thia[Br] or C_n Thia[Tf2N], with n = 2-16.

2.2. Spectroscopy

¹H, ¹³C and ¹⁹F NMR spectroscopy was performed on a JEOL 400 MHz NMR. NMR solvents were purchased from Cambridge isotope labs.

2.3. Physical properties

Melting points, glass transitions, and crystallization temperatures were measured using a TA instruments Q200 differential scanning calorimeter (DSC). Each sample was placed in an aluminum pan and cycled three consecutive times from $-90\,^{\circ}\text{C}$ to 150 $^{\circ}\text{C}$ at a heating and cooling rate of 10 $^{\circ}\text{C/min}$. Enthalpy values for the phase transitions were calculated using the TRIOS software from TA Instruments.

Decomposition temperatures were measured on a TA instruments Q500 thermogravimetric analyzer (TGA) using the default dynamic setting for the system and using a platinum pan. The differential thermogravimetric curves (DTG) were computationally obtained using the experimental TGA curves with OriginPro graph visualization software. Decomposition temperatures were taken from the minimum (maximum thermal decomposition rate) of each DTG curve.

Viscosity and density were measured using an Anton Paar SVM 3001 kinematic viscometer. Measurements were taken from 20 $^{\circ}\text{C}$ to 80 $^{\circ}\text{C}$ at increments of 5 $^{\circ}\text{C}$.

2.4. Single crystal and powder diffraction

Single crystals of C4-Thia[Br] and C16-Thia[Tf2N] were coated with a trace of Fomblin oil and were transferred to the goniometer head of a Bruker Quest diffractometer with kappa geometry, a Cu K α wavelength $(\lambda = 1.54178 \text{ Å})$ I- μ -S microsource X-ray tube, laterally graded multilayer (Goebel) mirror single crystal for monochromatization, a Photon II area detector, and an Oxford Cryosystems low temperature device. Examination and data collection were performed at 150 K. Data were collected, reflections were indexed and processed, and the files scaled and corrected for absorption using APEX3 [35] and SADABS [36]. The space groups were assigned and the structures were solved by direct methods using XPREP within the SHELXTL suite of programs [37,38] and refined by full matrix least squares against F^2 with all reflections using Shelxl2018 [39] using the graphical interface Shelxle [40]. H atoms were positioned geometrically and constrained to ride on their parent atoms. C—H bond distances were constrained to 0.95 Å for aromatic and alkene C—H moieties, and to 0.99 and 0.98 Å for aliphatic CH₂ and CH₃ moieties, respectively. Methyl H atoms were allowed to rotate but not to tip to best fit the experimental electron density. Uiso (H) values were set to a multiple of U_{eq}(C) with 1.5 for CH₃ and 1.2 for C—H and CH₂ units, respectively.

In C_{16} -Thia[TF₂N] the sulfur atom in the thiazolium fragments in both cations are disordered with a C—H group by rotation of the fragment. All disordered thiazolium moieties were restrained to have similar geometries. U^{ij} components of ADPs for disordered atoms closer to each other than 2.0 Å were restrained to be similar. Subject to these

conditions the occupancy ratio refined to 0.926(2) to 0.074(2) for the "A" cation, and to 0.786(2) to 0.214(2) for the "B" cation. One of the anions is disordered by a pseudo two-fold rotation. The disordered moieties were restrained to have similar geometries as the other not disordered anion. U^{ij} components of ADPs for disordered atoms closer to each other than 2.0~Å were restrained to be similar. Subject to these conditions the occupancy ratio refined to 0.8417(13) to 0.1583(13).

Complete crystallographic data, in CIF format, have been deposited with the Cambridge Crystallographic Data Centre. CCDC 2032481 and 2032482 contains the supplementary crystallographic data for this paper. These data can be obtained free of charge from The Cambridge Crystallographic Data Centre via www.ccdc.cam.ac.uk/data_request/cif.

Hirshfeld surfaces and images were calculated and produced using *CrystalExplorer17* [41]. Images of crystal structures and analysis of structures was accomplished using *Olex2* [42]. Predicted powder diffraction patterns were calculated using Mercury [43].

Powder X-ray Diffraction (PXPD) data were recorded on a Rigaku MiniFlex 600 X-ray diffractometer using the MiniFlex Guidance software. Samples were prepared on Rigaku zero background round flush sample holders. Measurements were made at 40 kV, 15 mA using Cu K α ($\lambda=1.5418$ Å) radiation at room temperature. The experimental parameters included a scan speed of 0.5°/min and a step size of 0.02° with regards to 20. The data were collected over the range of 3–50° with respect to 20.

3. Experimental

3.1. Formation of the ionic liquid compounds $C_2 - C_8$ -Thia $[Tf_2N]$

The appropriate alkyl bromide (1.2 equivalents) and thiazolium (1 equivalent) were added to a screw top vial. A stir bar was added to the vial and the vial was sealed with a lid. The mixture was heated at 90 °C for 3 days. After the 3 days, the reaction was cooled to room temperature during which a pale-brown solid formed. The resulting solid was triturated with diethyl ether and washed with ethyl acetate repeatedly until the liquid turned to clear. The cleaned solid was then dried under vacuum overnight and used without further purification.

The alkylated bromide salt (1 equivalent) was dissolved into a minimal amount of water and lithium bis(trifluoromethane)sulfonimide (1.2 equivalents) was added while stirring. The resultant mixture was stirred at room temperature for four hours after which the aqueous layer was decanted. The resultant organic phase was dissolved in dichloromethane and repeatedly washed with water in a separatory funnel. The solvent was removed in vacuo and the resultant pale-brown liquid was dried overnight under vacuum at 55 °C.

3.2. Formation of the ionic liquid compounds C_{12} & C_{16} -Thia $[TF_2N]$

The appropriate alkyl bromide (1.2 equivalents) and thiazolium (1 equivalent) were added to a screw top vial. A stir bar was added to the vial and the vial was sealed with a lid. The mixture was heated at 110 °C for 7 days. After the 7 days, the reaction was cooled during which a viscous brown liquid formed in the vials. Diethyl ether was added to the liquid and mixed until a brown solid formed. The solid was filtered and washed repeatedly with ethyl acetate. The cleaned solid was then dried under vacuum overnight and used without further purification.

The dodecyl or hexadecyl-alkylated bromide salt was dissolved into a minimal amount of warm water (60 °C). To this aqueous solution, 1.2 equivalents of lithium bis(trifluoromethane)sulfonimide, dissolved in a minimal amount of water, was added. The resultant mixture was stirred at 60 °C for 4 h after which the aqueous layer was decanted while warm. The resultant organic phase was dissolved in ethyl acetate and washed with water (3 \times 50 mL) in a separatory funnel. The solvent was removed in vacuo and the resultant pale brown liquid was dried overnight under vacuum at 55 °C.

3.3. 3-Ethyl-1,3-thiazol-3-ium bis(trifluoromethanesulfonyl)imide (C₂-Thia|Tf₂N|)

Pale yellow liquid. C₂-Thia[Tf₂N] remained as a liquid through all testing and experimental procedures. Yield (74%).

¹H NMR (400 MHz; Acetone–d₆) δ 10.20 (s, 1H), 8.62 (dd, J = 3.7, 1.0 Hz, 1H), 8.42 (t, J = 2.9 Hz, 1H), 4.82 (q, J = 7.3 Hz, 2H), 1.70 (t, J = 7.3 Hz, 3H).

¹³C NMR (101 MHz; Acetone–d₆) δ 158.19 (s, 1C), 137.19 (s, 1C), 126.46 (s, 1C), 120.12 (q, J = 321.1 Hz, 2C), 51.16 (s, 1C), 14.81 (s, 1C). ¹⁹F NMR (376 MHz; Acetone-d₆) δ – 79.79 (s, 6F).

3.4. 3-Butyl-1,3-thiazol-3-ium bromide (C_4 -Thia[Br])

Light brown powder. Yield (80%). Single crystals suitable for X-ray diffraction were grown by slow diffusion of diethyl ether into a saturated solution of ethanol.

¹H NMR (400 MHz; DMSO- d_6) δ 10.34 (s, 1H), 8.67 (t, J = 1.8 Hz, 1H), 8.39 (d, J = 2.3 Hz, 1H), 4.60 (t, J = 2.9 Hz, 2H), 1.85 (dd, J = 3.6, 1.8 Hz, 2H), 1.24 (s, 2H), 0.88 (dd, J = 4.1, 2.4 Hz, 3H).

¹³C NMR (101 MHz; DMSO- d_6) δ 150.31 (s, 1C), 128.95 (d, J = 5.3 Hz, 1C), 118.07 (d, J = 8.0 Hz, 1C), 47.00 (d, J = 4.1 Hz, 1C), 23.79 (s, 1C), 10.95 (s, 1C), 4.27 (s, 1C).

3.5. 3-Butyl-1,3-thiazol-3-ium bis(trifluoromethanesulfonyl)imide $(C_4$ -Thia $[Tf_2N^-]$)

Dark yellow liquid. Yield (68%).

¹H NMR (400 MHz; Acetone- d_6) δ 10.20 (t, J = 0.5 Hz, 1H), 8.60 (dd, J = 3.7, 1.0 Hz, 1H), 8.41 (t, J = 2.9 Hz, 1H), 4.76 (t, J = 7.5 Hz, 2H), 2.08 –2.01 (m, 2H), 1.39 (m, 2H), 0.93 (t, J = 7.4 Hz, 3H).

¹³C NMR (101 MHz; Acetone- d_6) δ 159.23 (s, 1C), 138.20 (s, 1C), 127.30 (s, 1C), 120.90 (q, J = 321.2 Hz, 2C), 56.27 (s, 1C), 32.82 (s, 1C), 19.95 (s, 1C), 13.55 (s, 1C).

¹⁹F NMR (376 MHz; Acetone- d_6) δ – 79.79 (s, 6F).

¹⁹F NMR (376 MHz; Acetone- d_6) δ – 79.76 (s, 6F).

3.6. 3-Hexyl-1,3-thiazol-3-ium bis(trifluoromethanesulfonyl)imide $(C_6$ -Thia $[T_5N])$

Dark yellow liquid. Yield (84%).

¹H NMR (400 MHz; Acetone- d_6) δ 10.18 (d, J=1.4 Hz, 1H), 8.59 (dd, J=3.7, 1.1 Hz, 1H), 8.40 (t, J=3.0 Hz, 1H), 4.75 (t, J=7.5 Hz, 2H), 2.10 –2.01 (m, 2H), 1.39–1.27 (m, 6H), 0.83 (dd, J=9.2, 4.9 Hz, 3H).

¹³C NMR (101 MHz; Acetone- d_6) δ 158.97 (s, 1C), 137.98 (s, 1C), 127.05 (s, 2C), 120.67 (q, J = 321.2 Hz, 2C), 56.27 (s, 1C), 31.45 (s, 1C), 30.62 (s, 1C), 26.11 (s, 1C), 22.70 (s, 1C), 13.86 (s, 1C).

3.7. 3-Octyl-1,3-thiazol-3-ium bis(trifluoromethanesulfonyl)imide $(C_8$ -Thia $[Tf_2N])$

Pale yellow liquid. Yield (81%).

¹H NMR (400 MHz; Acetone- d_6) δ 10.19 (d, J = 1.3 Hz, 1H), 8.60 (dd, J = 3.7, 1.0 Hz, 1H), 8.41 (t, J = 3.0 Hz, 1H), 4.76 (t, J = 7.5 Hz, 2H), 1.38 –1.22 (m, 12H), 0.82 (t, J = 6.8 Hz, 3H).

 $^{13}\mathrm{C}$ NMR (101 MHz; Chloroform-*d*) δ 157.24 (s, 1C), 137.13 (s, 1C), 126.18 (s, 1C), 119.78 (q, J=321.0 Hz, 1C), 56.29 (s, 1C), 31.60 (s, 1C), 30.33 (s, 1C), 28.90 (s, 1C), 28.75 (s, 1C), 25.98 (s, 1C), 22.55 (s, 1C), 14.01 (s, 1C).

¹⁹F NMR (376 MHz; Acetone- d_6) δ – 79.77 (s, 6F).

3.8. 3-Dodecyl-1,3-thiazol-3-ium bis(trifluoromethanesulfonyl)imide $(C_{12}$ -Thia $[Tf_2N])$

Pale yellow liquid which slowly solidified upon resting at room temperature overnight. Yield (88%).

¹H NMR (400 MHz; Acetone- d_6) δ 10.17 (d, J = 1.7 Hz, 1H), 8.58 (dd, J = 3.7, 1.2 Hz, 1H), 8.39 (dd, J = 3.5, 2.6 Hz, 1H), 4.74 (t, J = 7.5 Hz, 2H), 1.38–1.26 (m, 20H), 0.82 (t, J = 6.8 Hz, 3H).

¹³C NMR (101 MHz; Chloroform) δ 157.47 (s, 1C), 137.12 (s, 1C), 126.19 (s, 1C), 119.85 (q, J=321.0 Hz, 1C), 56.40 (s, 1C), 32.00 (s, 1C), 30.44 (s, 1C), 29.68 (s, 1C), 29.65 (s, 1C), 29.53 (s, 1C), 29.42 (s, 1C), 29.35 (s, 1C), 29.90 (s,1C), 26.11 (s, 1C), 22.78 (s, 1C), 14.21 (s, 1C). ¹⁹F NMR (376 MHz; Acetone- d_6) δ - 79.73 (s, 6F).

3.9. 3-hexadecyl-1,3-thiazol-3-ium bis(trifluoromethanesulfonyl)imide $(C_{16}$ -Thia[Tf2N])

Pale yellow crystalline solid. Yield (87%).

Single crystals suitable for X-ray diffraction were grown by slow evaporation of a saturated solution of the compound dissolved in methanol.

¹H NMR (400 MHz; Acetone- d_6) δ 10.23 (dd, J = 2.0, 1.6 Hz, 1H), 8.63 (dd, J = 3.7, 1.3 Hz, 1H), 8.43 (dd, J = 3.6, 2.5 Hz, 1H), 4.78 (t, J = 7.5 Hz, 2H), 1.39–1.24 (m, 28H), 0.84 (t, J = 6.8 Hz, 3H).

¹³C NMR (101 MHz; Chloroform-*d*) δ 157.52 (s, 1C), 137.09 (s, 1C), 126.20 (s, 1C), 119.86 (q, J = 321.1 Hz, 1C), 56.42 (s, 1C), 32.04 (s, 1C), 30.46 (s, 1C), 29.82 (s, 3C), 29.78 (s, 1C), 29.76 (s, 1C), 29.57 (s, 1C), 29.49 (s, 1C), 29.38 (s, 1C), 28.93 (s, 1C), 26.13 (s, 1C), 22.81 (s, 1C), 14.24 (s, 1C).

¹⁹F NMR (376 MHz; Acetone- d_6) δ – 79.79 (s, 6F).

4. Results and discussion

4.1. Thermal stability

A summary of the measured physicochemical properties is given in Table 1. Thermogravimetric analysis (TGA) and calculated derivative (DTG) curves of all seven compounds are shown in Fig. 1. Compounds C₁₂-Thia[Tf₂N] and C₁₆-Thia[Tf₂N] displayed similar decomposition profiles characterized by a single decomposition step with no residual carbonaceous material remaining. Compounds C2-Thia[Tf2N], C4-Thia [Tf₂N], C₆-Thia[Tf₂N], and C₈-Thia[Tf₂N], on the other hand, show an initial decomposition step at approximately 350 °C followed by a second step at higher temperatures ranging from 400 °C to 450 °C. For example, the TGA trace for C₂-Thia[Tf₂N] shows two decomposition steps, the first starts at 353 °C, with a loss of 95% and the second decomposition begins at 433 °C wherein the remaining mass is lost. The relative percentages of mass lost for the C2 through C8 compounds at each step is similar indicating that the first major step in the decomposition mechanism is identical for the compounds despite the varying alkyl chain length. Overall, C_2 -Thia $[Tf_2N]$ has the highest T_{dec} for all the compounds examined while C_4 -Thia[Br] had the lowest.

It was found that T_{dec} and alkyl chain length are inversely related. Consistently, as alkyl chain length increases, the ionic liquid decomposes at a lower temperature. The decomposition temperature of ILs is

an important property, as it reflects the thermal stability and ability to be used for PCMs applications. All the decomposition temperatures of the thiazolium-based IL compounds are higher than 200 °C; this property can meet the requirements of commercial PCMs such as Therminol VP-1 and paraffin, which are used as heat transfer and storage materials industrially [44,45].

Compared to structurally related imidazolium-based ILs, thiazolium ILs display lower thermal stability and more complex decomposition pathways. The imidazole containing ILs, namely 1-ethyl-3-methylimidazolium [Tf₂N $^-$], or simply [C₂Mim][Tf₂N] (T_{dec} 440 °C) [46], and 1-butyl-3-methylimidazolium Tf₂N, or [C₄Mim(Tf₂N)] (T_{dec} 439 °C) [14], both display higher thermal stability as compared to the thiazolium-based ILs. Compounds C₂-Thia[Tf₂N], and C₄-Thia[Tf₂N] decomposed at approximately 100 °C less than its imidazolium congener. This significant change in thermal stability implicates that the thiazolium ring is likely the point of decomposition.

Compared to the $[Tf_2N^-]$ bearing compounds, the halide compound C_4 -Thia[Br] has the lowest decomposition temperature at 203 °C. As has been examined previously in the literature, halide-based compounds exhibit reduced thermal stability since the anions have higher nucleophilic and basic character [1,17,47,48], C_4 -Thia[Br] does display a similar TGA profile as compared to C_{12} -Thia $[Tf_2N]$ and C_{16} -Thia $[Tf_2N]$ characterized by a single decomposition step. As a point of comparison, C_4 -ThiaBr has a T_{dec} approximately 70 °C less than the imidazolium congener C_4 -Mim[Br] ($T_{dec} = 273$ °C) [19].

4.2. Phase transitions

Phase transitions for the ILs were examined by DSC and the results are summarized in Table 1. Selected DSC curves are shown in Fig. 1 **(C)**. All compounds displayed consistent DSC profiles over three consecutive heating and cooling cycles (see **Supplemental Information**). Compounds C_2 -Thia[Tf_2N], C_4 -Thia[Br], C_{12} -Thia[Tf_2N], and C_{16} -Thia [Tf_2N] have distinct melting and freezing points. Although supercooling of ILs is common, C_4 -Thia[Br], C_{12} -Thia[Tf_2N], and C_{16} -Thia[Tf_2N] readily crystallize and do not exhibit any glass transitions, a favorable property for PCMs [9,11]. C_{12} -Thia[TF_2N], C_{16} -Thia[TF_2N], and C_4 -Thia[TF_1] had well-defined peaks with large heat of fusion values potentially making them viable PCMs for heat storage applications.

4.3. Viscosity

The densities and the temperature dependency for C_n -Thia[Tf₂N], n=2,4,6 and 8 compounds are presented in Fig. 2 **(A)**, and also summarized in Table 1 for values measured at 25 °C. These results also include the linear fittings for the experimental data points. The density of C_2 -Thia[Tf₂N] has the highest values at all investigated temperatures. This parameter decreases systematically with increasing the alkyl chain length. Such trends may be explained by the greater increase in the molecular volume of the cation as compared to only small increases in

Table 1 Summary of physicochemical properties for C_n -Thiazolium based ionic liquids.

Compound	MW [g/mol] ^a	Density [g/cm ³] ^b	\overline{V} [cm ³ /mol] ^c	$T_m [^{\circ}C]^d$	$\Delta H_m [J/g]^e$	$\Delta H_{CC} [J/g]^f$	$T_{dec} [^{\circ}C]^{g}$	η [mPa.s] h	E_a [kJ/mol] ⁱ
C ₂ -Thia[Tf ₂ N]	394.34	1.62	243.42	30	29.62	24.35	356	65	26.9 ± 0.4
C_4 -Thia $[Tf_2N]$	422.40	1.51	279.74	-	-	-	341	90	30.6 ± 0.5
C_6 -Thia $[Tf_2N]$	450.45	1.46	308.53	16	13.43	15.53	339	181	36.0 ± 0.7
C_8 -Thia $[Tf_2N]$	478.50	1.39	344.24	-	-	-	337	225	37.4 ± 0.6
C_{12} -Thia $[Tf_2N]$	534.61	-	-	32	64.25	63.38	334	-	-
C_{16} -Thia $[Tf_2N]$	590.72	-	-	57	74.17	79.19	331	-	-
C ₄ -Thia[Br]	222.15	-	-	135	112.62	105.11	203	-	-

a Molecular weight bensity measured at 25 °C; °Molar volume of compounds at 25 °C; dMelting temperature from DSC curves; Enthalpy of fusion calculated from integration of DSC melting peak transitions; fEnthalpy of cold crystallization from DSC traces; Decomposition temperatures from the minimum of the DTG curves corresponding to the main decomposition step in the TG profiles; Dynamic viscosity measured at 25 °C; Activation energy for dynamic viscosity from Andrade plot fittings, with uncertainties estimated from the linear fitting errors.

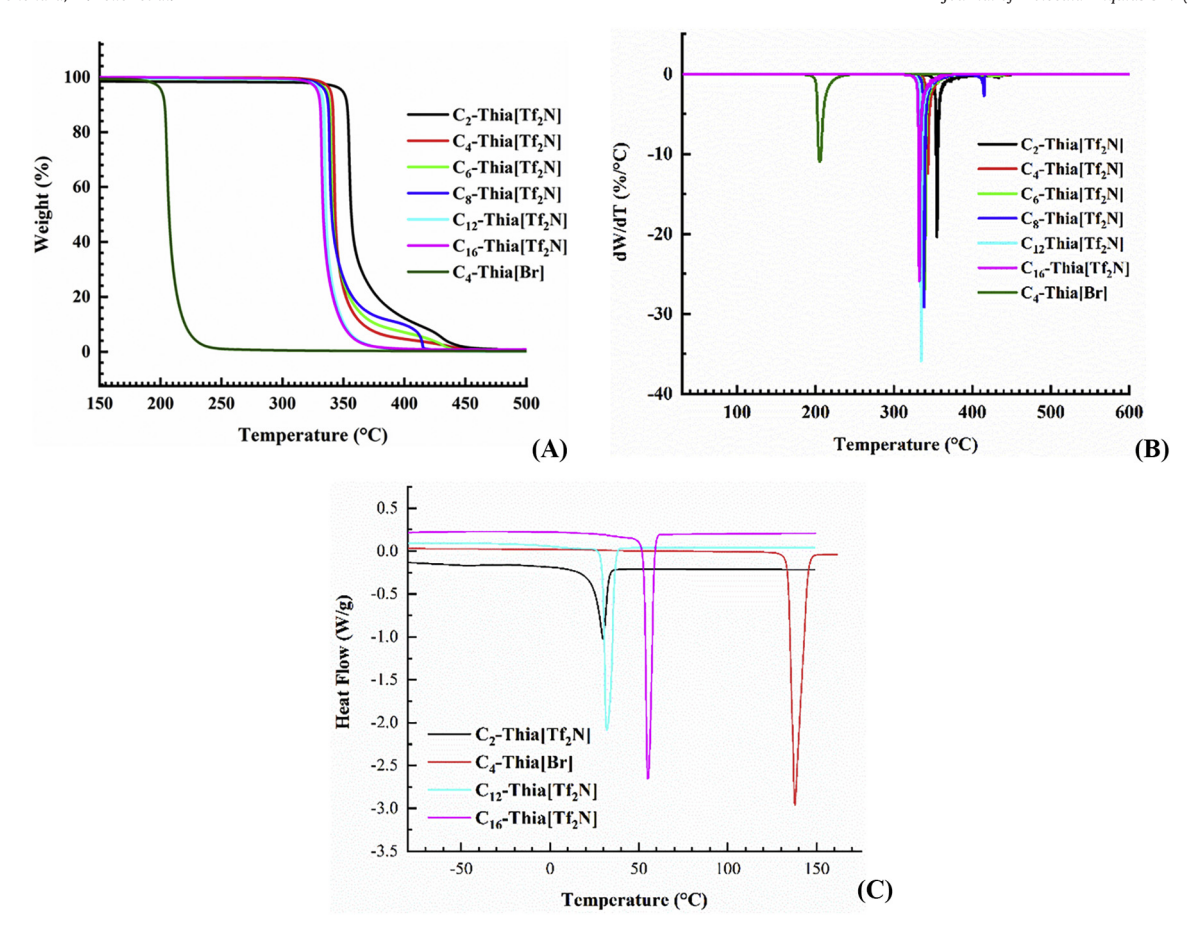


Fig. 1. TGA (A) and calculated DTG (B) curves for the C_n -Thia[Tf₂N] compounds, with n=2,4,6,8,12 and 16 and for C_4 -Thia[Br]. DSC curves showing a single heating cycle for selected compounds (C).

molecular weight. Moreover, the dynamic viscosity values, see Fig. 2 **(B)**, follow the opposite trend, with increasing molecular weight of the compounds leading to higher viscosities. The increase in viscosity is primarily a consequence of non-covalent forces in the series of compounds. For instance, compound C_2 -Thia[Tf₂N] had the lowest viscosity at 25 °C (65 mPa.s), and C_8 -Thia[Tf₂N] displayed the highest viscosity at the same temperature (225 mPa.s). This trend, as seen in Fig. 2 **(C)**, is maintained for the kinematic viscosity, which is given by the ratio between the dynamic viscosity and the density. In general, the thiazolium-based ILs display higher viscosity values compared to their imidazolium analogues. For example, [C₄-Mim][Tf₂N] has a viscosity value of 69 mPa.s at 25 °C¹⁵ which is 32% lower than the viscosity of compound C_4 -Thia[Tf₂N].

The temperature dependent viscosity (η) has been fitted to the Andrade equation and the profiles for C_2 -Thia[Tf $_2$ N], C_4 -Thia[Tf $_2$ N], C_6 -Thia[Tf $_2$ N], and C_8 -Thia[Tf $_2$ N] from 20 °C to 80 °C are shown in Fig. 2 (**D**). The Andrade equation is

$$\eta = \eta_0 \exp\left[B/T\right] \tag{1}$$

Where η_0 (mPa.s) and the activation energy (E_a) and the ideal gas constant (R) are given by the parameter $B=E_a/R$. The positive sign for the exponential indicates that viscosity decreases with increasing temperature, but the process is activated. The values of E_a are approximately 27 kJ/mol for C₂-Thia[Tf₂N] and 37 kJ/mol for C₈-Thia[Tf₂N]. These values correspond to approximately the energy for H-bond interactions [49]. The small increase in energy with increasing alkyl chain probably results from the increase in non-covalent intermolecular forces. Overall, the linear fit indicates an Arrhenius-type behavior for

the viscosities, which agrees with previously reported thiazolium-based ILs [30].

4.4. Solid-state structures

The crystal structures of C₄-Thia[Br] and C₁₆-Thia[Tf₂N] were obtained and their structures are shown in Fig. 3. With respect to the structure of the C₁₆-Thia[Tf₂N] compound, there are two sets of ion pairs in the asymmetric unit. The thiazolium ring portions of the structures are positionally disordered in two parts, with the sulfur atom occupying the position of a carbon atom and vice-versa. Further, one of the Tf₂N⁻ anions is disordered. Both cations in the C₁₆-Thia[Tf₂N] structure have the same orientation of the alkyl chains, with the chains running in parallel. The orientation of the alkyl chains, with respect to the thiazolium core in both crystal structures, is similar to other examples in the literature [50]. The torsion angle of atoms C2-N1-C6-C7, which describes the orientation of the alkyl chain, in both cation moieties within the $[Tf_2N^-]$ structure is 106.2(14)° and 103.15(15)°. This orientation of alkyl chains is also observed in the C₄-Thia[Br] structure wherein the related torsion angle is 108.2(9)°. This observation leads to the conclusion that the alkyl chain configurations are independent of chain length and perhaps even the anion. Previous literature discussion points to the possibility of polymorphs of the structures existing wherein the alkyl chains would exhibit different rotational configurations [50].

To further understand the structures in the solid state, powder X-ray diffraction (pXRD) data was collected on both samples. The predicted pXRD patterns were calculated from the single crystal data sets and compared with the experimental patterns (see Fig. 4). In general, the

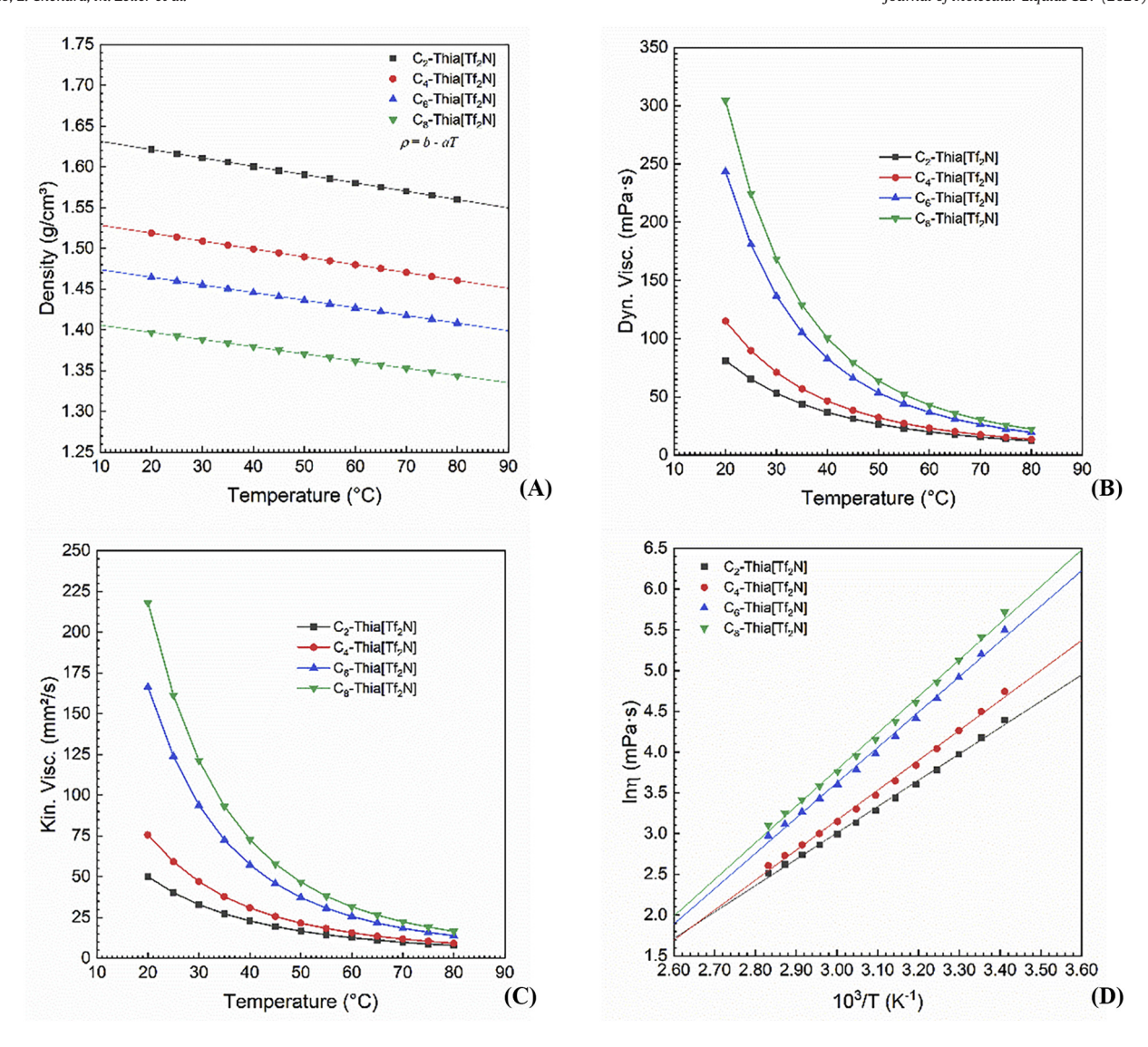
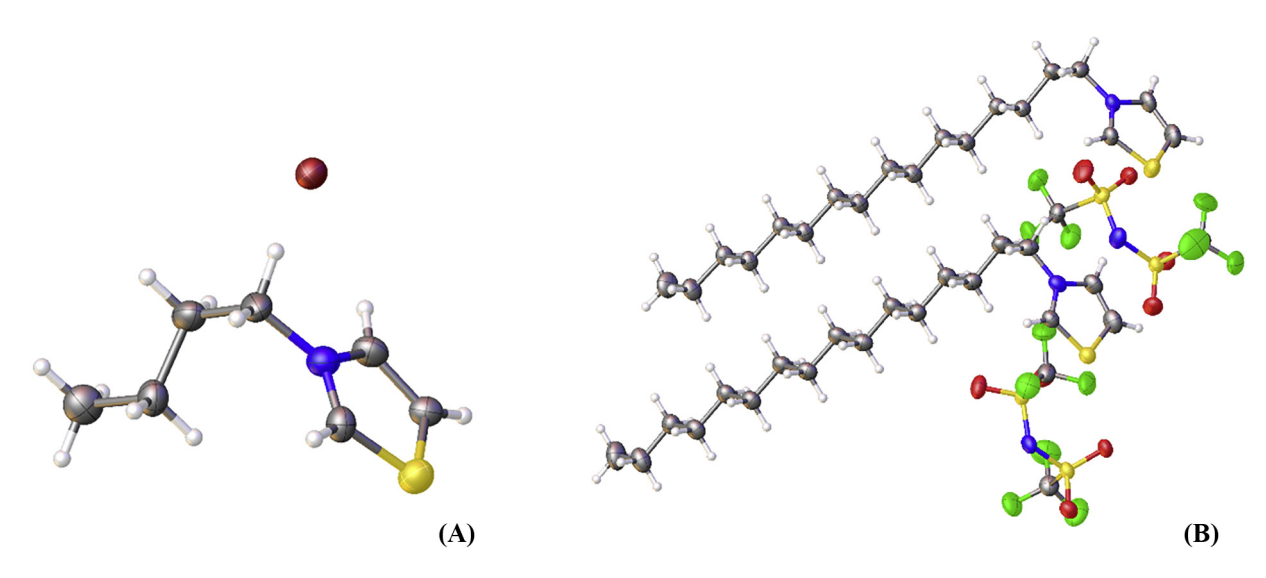
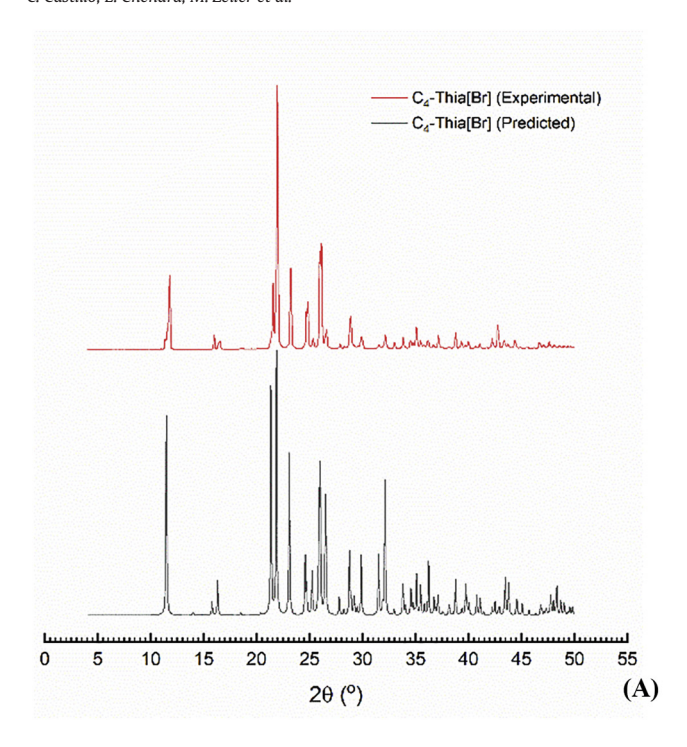


Fig. 2. Temperature dependency of density (A), dynamic (B) and kinematic viscosity (C) for C_n -Thia[Tf₂N], n = 2, 4, 6 and 8 compounds. Fittings of the dynamic viscosity according to the Andrade model (D).



 $\textbf{Fig. 3.} \ Crystal \ structures \ of \ C_4-Thia[Br] \ \textbf{(A)} \ and \ C_{16}-Thia[Tf_2N] \ \textbf{(B)} \ shown \ with 50\% \ probability \ ellipsoids. The \ disordered portions of the cations and anions in the \ C_{16}-Thia[Tf_2N] \ structure \ are \ omitted \ for \ clarity. \ Carbon = gray, \ nitrogen = blue, \ fluorine = green, \ oxygen = bright \ red, \ sulfur = yellow, \ hydrogen = white, \ bromide = dark \ red.$



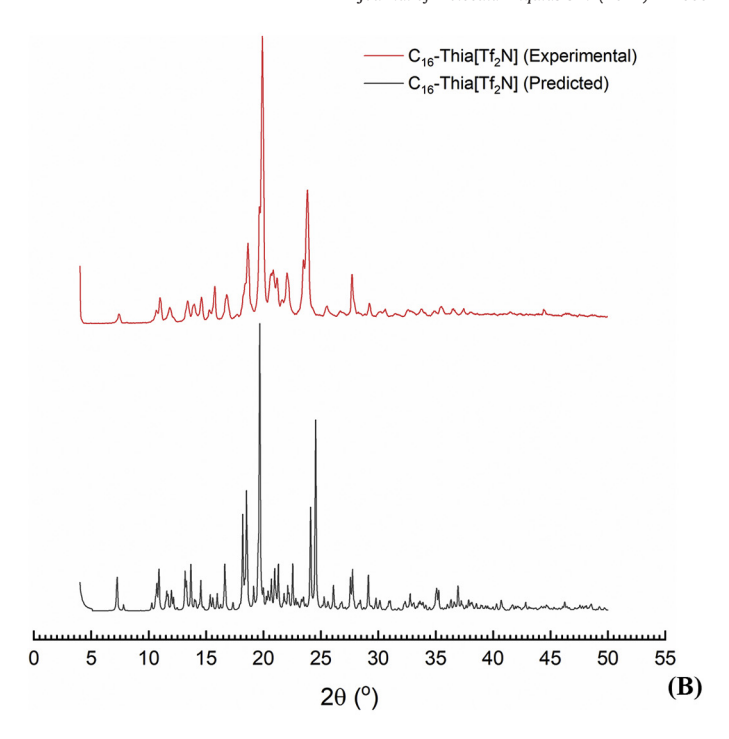


Fig. 4. Experimental and simulated XRD patterns for C₄-Thia[Br] (A) and C₁₆-Thia[Tf₂N] (B).

experimental and predicted XRD data matches closely indicating that the solid-state structures for both samples are similar in the crystalline state as in the polycrystalline powdered form, and that no phase change is observed between the temperature of single crystal data collection (150 K) and ambient conditions, under which the powder patterns were obtained. This provides evidence that the configurations and structures discussed herein are likely the preferred structures for these ILs. Screening of samples crystallized through different methods and solvents yielded identical unit cells for C₄-Thia[Br] and all crystal samples looked similar by visual inspection under the microscope indicating that the two compounds are not prone towards polymorph formation.

The thiazolium-based crystal structures reported herein represent some of the few examples reported in the literature to date. Thus, to better understand the overall solid-state structure of the compounds as well as differing intramolecular interactions of the two crystal structures, a Hirshfeld surface analysis was performed on both samples [51]. In brief, Hirshfeld surface analysis involves examining intermolecular interactions "through a whole molecule approach." [52] Visualization of intermolecular interactions can be accomplished through 2D fingerprint plots which can be deconstructed to examine relative percentages of contribution to the overall interactions on an elemental basis [53]. The values d_i and d_e refer to distances from the Hirshfeld surface to a nucleus inside (d_i) or to a nucleus outside (d_e) . In this analysis, d_{norm} is a normalized function of d_i and d_e [54].

With respect to the disordered cationic portion of the C_{16} -Thia $[Tf_2N]$ structure, surface analysis was performed on both orientations of the disorder for both cations as a whole. The C_4 -Thia[Br] structure was compared to the previously reported imidazolium congener 1-butyl-3-methylimidazolium bromide or C_4 -Mim[Br] [23]. Fingerprint plots of the intermolecular interactions are shown in Fig. 5 and the Hirshfeld surfaces mapped with the normalized contact distance d_{norm} and the shape index are shown in Fig. 6. Individual percentages of relevant interactions are listed in Table 2 for both the C_4 -Thia[Br] and C_4 -Mim[Br] structures.

As seen in Table 2, both the C_4 -Thia and C_4 -Mim cations share similar percentages of $H\cdots Br$ and $H\cdots C$ interactions. One distinction arises

from the H···H interactions wherein the C₄-Mim[Br] structure has a significantly higher percentage than the thiazolium congener. Further, by examining the fingerprint plots it is evident that there are significant differences in the nature of these H···H interactions. The C₄-Mim[Br] structure has a defined H···H peak at approximately $d_i = d_e \approx 1.2$ Å with the surrounding area showing continuous, dense interactions. The C₄-Thia[Br] structure, however, shows a broader range of H···H interactions with disperse spots and a broadened peak. This observation is in contrast to the melting points for the two structures wherein the C₄-Thia[Br] melts at a significantly higher temperature (135 °C) as compared to the C₄-Mim[Br] (~79 °C) [55]. It follows then that the H···H interactions are not the dominating intermolecular forces influencing the melting points despite constituting the highest overall percentage of interactions.

Both sets of crystals exhibit defined $H \cdots Br$ peaks observed in the fingerprints. In both crystals the bromide ion shows the shortest interactions with hydrogens on the heterocyclic ring. In C_4 -Mim[Br] the shortest interaction is with the central C2—H hydrogen, d = 2.45(6)Å. The thiazolium structure, however, has the shortest interaction with C5—H, d = 2.80(7)Å. The C2—H···Br interaction in C₄-Thia is significantly longer (d = 2.93(8) Å) when compared with the imidazolium congener. The rest of the $C-H\cdots Br$ interactions from the hydrogens on the rings are similar in the two compounds, with distances of approximately 2.9 Å. These interactions account for the comparable shapes in the $H\cdots Br$ spike in both fingerprints. As with the discussion of the $H \cdots H$ interactions, the difference in the $H \cdots Br$ interactions of the two structures does not appear to account for the significant difference in the melting points. Simply examining the hydrogen bonding interactions would lead to the conclusion that the C_4 -Thia[Br] structure would have a similar, or perhaps lower, melting point based on the longer interactions. However, this is clearly not the case in the thiazolium-compounds nor in ionic liquids in general. There is a more complex relationship between melting point and intermolecular interactions which cannot be solely predicted from hydrogen bonding [17,56].

The C_4 -Mim[Br] structure exhibits a higher percentage of $H \cdots N$ | $N \cdots H$ reciprocal interactions wherein hydrogen atoms on symmetry

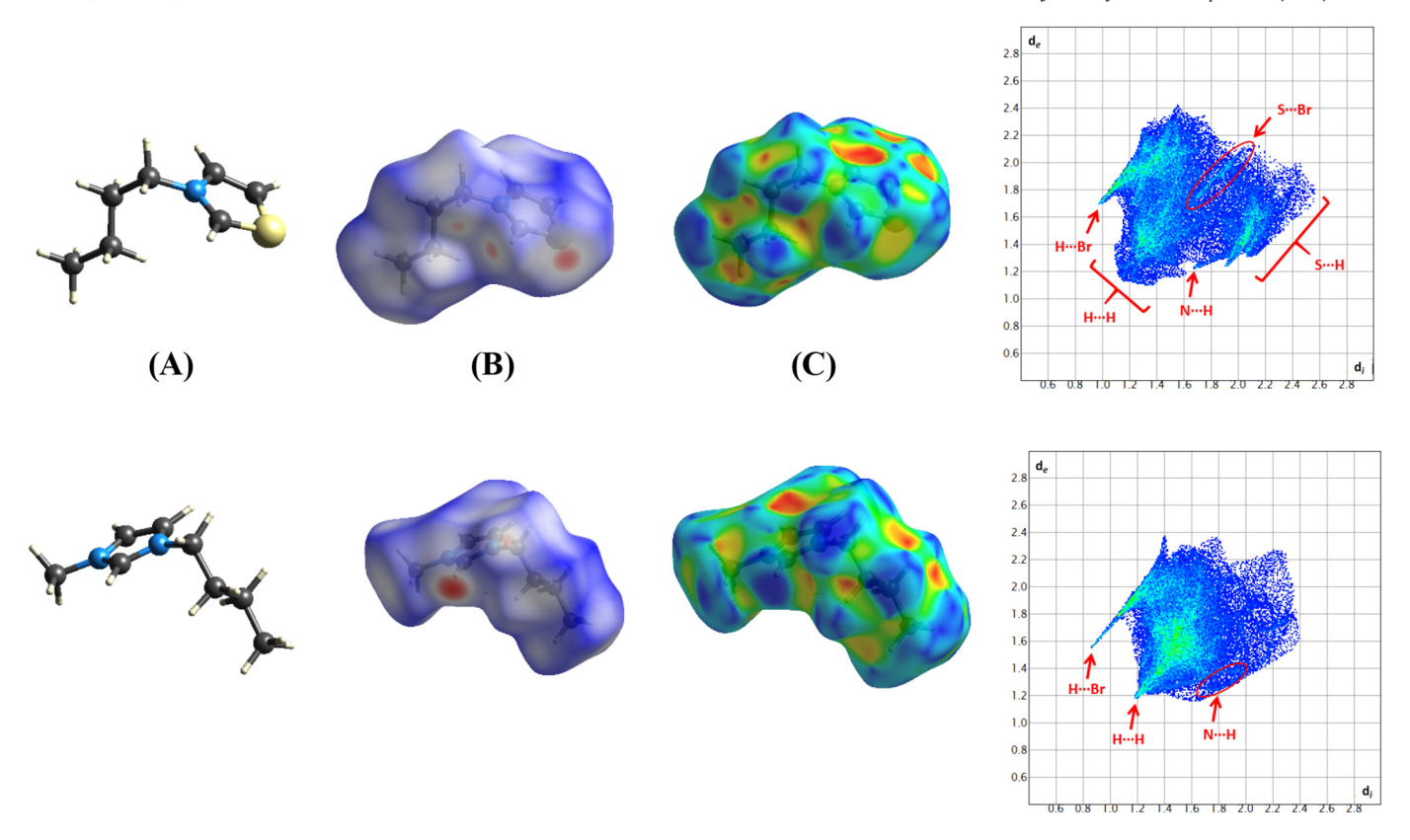


Fig. 5. C_4 -Thia cation from the crystal structure (top). The Hirshfeld surfaces mapped with $d_{norm}(\mathbf{B})$ and the shape index (**C**) are shown along with a representation of the structure with no mapping as reference (**A**). The cation from the C_4 -Mim[Br] structure along with the mapped surfaces are shown (bottom). Fingerprint plots for both cations are shown at the far right.

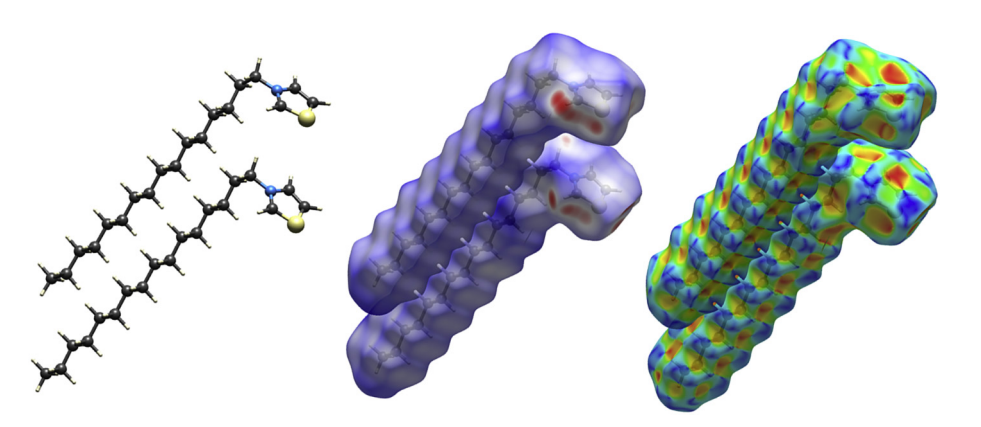


Fig. 6. Both cations from the asymmetric unit of the crystal structure of C_{16} -Thia[Tf₂N]. The cations with the Hirshfeld surfaces mapped with d_{norm} and the shape index are shown to the middle and right respectively. Only one part of the disorder in the cations is shown for clarity.

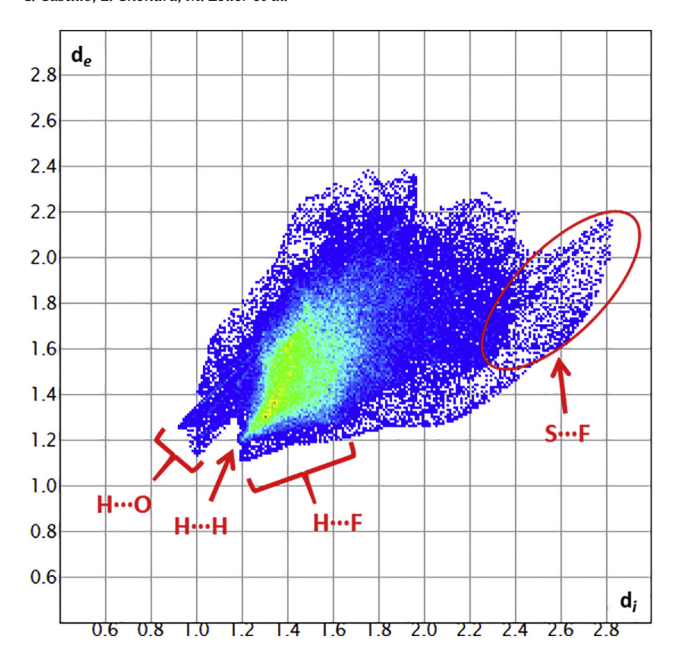
adjacent cations are interacting with the nitrogen atoms in the ring. These interactions arise from a set of alkyl chains sitting above one face of the ring, with the closest interactions coming from the methylene group (C9) and methyl group (C10). The thiazolium structure

Table 2 Percentages of interactions between atoms in the solid-state arising from the cations in C_4 -Thia[Br] and C_4 -Mim[Br].

Cation	H···All	н…н	H···Br	H···N N···H	H···C C···H	H···S S···H	S···Br
C ₄ -Thia	79.5	56.2	12.5	2.2	10.1	17.4	1.6
C ₄ -Mim	92.7	75.0	12.2	4.0	8.5	-	

does display a similar interaction, with the terminal methyl group (C9) interacting with the nitrogen on the ring. Naturally thiazolium contains one less nitrogen in the ring which would reduce the overall contribution of these interactions, however the presence of this alkyl-cation interaction in both systems indicates an important intermolecular interaction not affected by the atomic composition of the heterocycle ring. For both structures the point interaction is clearly seen as the red indentations when examining the shape index mapped over the Hirshfeld surfaces as seen in Fig. 5 [57].

The most significant difference between the two structures comes from interactions from the sulfur atom. A 'wing' type feature, as well as a smaller spike, of disperse spots arising from $S\cdots H$ interactions is seen in the indicated region in the fingerprint for C_4 -Thia[Br]. The



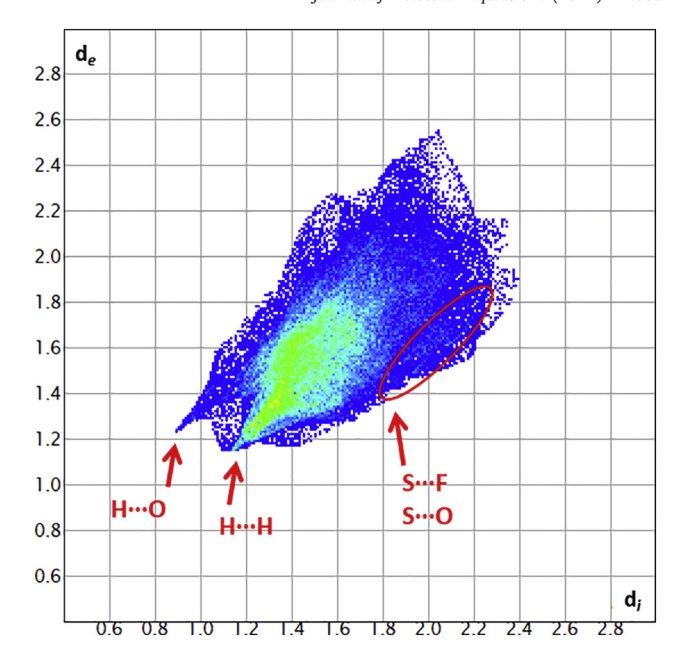


Fig. 7. Fingerprint plots for both cations A (left) and B (right) in the asymmetric unit of the C_{16} -Thia[Tf₂N] crystal structure.

reciprocal set of interactions, that is $H\cdots S$, is buried within the larger bulk of the interactions at their respective d_i and d_e ranges. The shortest interactions, represented by the spike, arise from the hydrogen atoms on the methylene carbon (C8) interacting with the sulfur at a distance of approximately 3.4 Å. Longer interactions with methyl carbons sitting above and below the plane of the rings interact at distances of approximately 3.5 Å. These $H\cdots S$ interactions can be seen as the yellow indentations on the shape index. Finally, the sulfur and bromide ion are interacting is a σ -hole type interaction with distances of 3.454(2) Å to 3.798(2) Å to the nearest symmetry equivalent bromide ions [58,59]. As discussed in the literature, these σ -hole interactions can have significant impact on the overall properties of molecules, including melting points [60].

The complex relationship of hydrogen bonding in ionic liquids and their impacts on the physical properties of the compounds is a continuing area of study [61]. In brief, the symmetry, geometry, and composition of both the cations and anions have a large impact on the strength and type of hydrogen interactions present within ILs [1,56,61]. Drawing conclusions based on discussions from the relevant literature, it is evident that overall the C₄-Thia[Br] compound exhibits several of the expected cation-anion interactions, both with the heterocycle and the alkyl side chain. However, more experimental crystal structures coupled with in-depth computational analysis will be required to establish a firm understanding of the impacts of the sulfur interactions on the solid-state structure of thiazolium-based ILs.

The fingerprint plots and mapped surfaces for both of the cations found in the asymmetric unit of the C_{16} -Thia[TF₂N] crystals are shown in Figs. 6. While both cations display similar interactions the fingerprint plots do highlight some key differences. One difference arises from the local disorder of the [Tf₂N $^-$] anions closest to cation A. This positional disorder of the anion gives rise to the disperse set of S \cdots F interactions. Despite the disorder, cation B shows more well-defined S \cdots O and S \cdots F interactions with a green spike for both indicated in Fig. 7. In both structures, however, H \cdots H interactions from the alkyl chains comprise the largest percentage of the total interactions and are easily seen as the dense, bright green regions in both plots. Interactions from the stacked alkyl chains are clearly seen when examining the shape index mapped on the Hirshfeld surface.

Interactions between the cation and anions in C_{16} -Thia[Tf₂N] display interesting distinctions when compared with the C_4 -Thia[Br] structure. Interactions with the central imide nitrogen of the anion shows the

shortest interactions C5—H in both cations with approximate distances of 2.5 Å. The C2—H hydrogen shows the shortest overall cation—anion interactions at approximately 2.3 Å.

Examining all three of the thiazolium containing cations, that is the cation from C_4 -Thia[Br] and the two within C_{16} -Thia[Tf₂N], it is evident that more long-distance interactions are present when compared to the imidazolium-based structure discussed herein. Interactions with the thiazoliums are consistently seen up to 2.6 Å in both d_i or d_e , and in the case of cation A in the C_{16} -Thia[Tf₂N] structure are seen up to 2.8 Å. However, similarities in interactions are also noted as the heterocycle hydrogens are prominent points of interactions in all cases.

5. Conclusions

Seven novel ionic compounds were synthesized, and their thermal and physical properties analyzed. Three of the compounds were shown to have favorable properties with potential application to PCMs. Solid-state characterization of the compounds helped to reveal the impact of the sulfur atom in the thiazolium ring has on the overall properties of the ILs, both in the solid state and in the liquid state. Non-covalent interactions with the alkyl chains on adjacent cations as well as σ -hole interactions with anions originating from the sulfur atom are theorized to account for the higher enthalpies observed in the phase transitions. While thermal stabilities of the compounds are lower than the imidazolium congeners, four of the compounds do exist as room temperature ionic liquids, and two additional compounds have melting points below 100 °C. Moreover, while activation energies for viscosity match those expected for hydrogen-bonds, especially between cations, these σ -hole interaction forces between cations and anions may play an additional role in the non-covalent forces dictating the increasing trend with molecular weights. Such σ -hole interactions may help modulate the strength of H-bonds in the series of investigated compounds having linear alkyl side chains. Further studies are ongoing to continue to study the structural impact and biological application of thiazolium-based ILs. Besides the enhanced biocompatibility of thiazolium cations over less expensive imidazolium-based compounds, knowledge of these intermolecular forces and of the resulting physicochemical properties of these novel thiazolium ionic liquids may lead to tailored properties for biomedical, energy, and synthetic applications.

Funding

This work was supported by Ave Maria University Department of Chemistry and Physics; Part of this material is based upon work supported by the National Science Foundation through the Major Research Instrumentation Program under Grant No. CHE 1530959, 1919785 and 1625543.

CRediT authorship contribution statement

Christine Castillo: Methodology, Resources, Investigation. Erica Chenard: Methodology, Resources, Investigation. Matthias Zeller: Investigation, Writing - review & editing. Nahla Hatab: Writing - review & editing, Formal analysis. Pasquale F. Fulvio: Data curation, Investigation, Writing - original draft, Writing - review & editing, Formal analysis. Patrick C. Hillesheim: Conceptualization, Methodology, Validation, Formal analysis, Supervision, Funding acquisition, Project administration, Writing - original draft, Writing - review & editing.

Declaration of Competing Interest

This manuscript is of novel work and has not been submitted elsewhere for consideration. Further, all authors have approved the article and are aware of its submission and agree to the policies set forth by your journal and its publishing company. There are no conflicts of interest to report from any authors.

References

- Fundamentals of Ionic Liquids; Wiley-VCH Verlag GmbH & Co. KGaA: Weinheim, Germany. 2017. doi:https://doi.org/10.1002/9783527340033.
- [2] C.P. Mehnert, R.A. Cook, N.C. Dispenziere, M. Afeworki, Supported ionic liquid catalysis a new concept for homogeneous Hydroformylation catalysis, J. Am. Chem. Soc. 124 (44) (2002) 12932–12933, https://doi.org/10.1021/ja0279242.
- [3] M. Galiński, A. Lewandowski, I. Stępniak, Ionic Liquids as Electrolytes, Electrochim. Acta 51 (26) (2006) 5567–5580, https://doi.org/10.1016/j.electacta.2006.03.016.
- [4] Q. Yang, Z. Zhang, X.-G. Sun, Y.-S. Hu, H. Xing, S. Dai, Ionic Liquids and derived materials for Lithium and sodium batteries, Chem. Soc. Rev. 47 (6) (2018) 2020–2064, https://doi.org/10.1039/C7CS00464H.
- [5] M. Aghaie, N. Rezaei, S. Zendehboudi, A systematic review on CO2 capture with ionic Liquids: current status and future prospects, Renew. Sust. Energ. Rev. 96 (2018) 502–525, https://doi.org/10.1016/j.rser.2018.07.004.
- [6] J.L. Shamshina, O. Zavgorodnya, H. Choudhary, B. Frye, N. Newbury, R.D. Rogers, In search of stronger/cheaper chitin Nanofibers through electrospinning of chitincellulose composites using an ionic liquid platform, ACS Sustain. Chem. Eng. 6 (11) (2018) 14713–14722, https://doi.org/10.1021/acssuschemeng.8b03269.
- [7] S. Gillet, M. Aguedo, L. Petitjean, A.R.C. Morais, A.M. da Costa Lopes, R.M. Łukasik, P.T. Anastas, Lignin transformations for high value applications: towards targeted modifications using green chemistry, Green Chem. 19 (18) (2017) 4200–4233, https://doi.org/10.1039/C7GC01479A.
- [8] K. Pielichowska, K. Pielichowski, Phase change materials for thermal energy storage, Prog. Mater. Sci. 65 (2014) 67–123, https://doi.org/10.1016/j.pmatsci.2014.03.005.
- [9] K. Matuszek, R. Vijayaraghavan, C.M. Forsyth, S. Mahadevan, M. Kar, D.R. MacFarlane, Pyrazolium phase-change materials for solar-thermal energy storage, ChemSusChem 13 (1) (2020) 159–164, https://doi.org/10.1002/cssc.201902601.
- [10] D.R. MacFarlane, N. Tachikawa, M. Forsyth, J.M. Pringle, P.C. Howlett, G.D. Elliott, J.H. Davis, M. Watanabe, P. Simon, C.A. Angell, Energy applications of ionic Liquids, Energy Env. Sci 7 (1) (2014) 232–250, https://doi.org/10.1039/C3EE42099J.
- [11] K. Matuszek, R. Vijayaraghavan, M. Kar, D.R. MacFarlane, Role of hydrogen bonding in phase change materials, Cryst. Growth Des. 20 (2) (2020) 1285–1291, https://doi. org/10.1021/acs.cgd.9b01541.
- [12] N. Terasawa, S. Tsuzuki, T. Umecky, Y. Saito, H. Matsumoto, Alkoxy chains in ionic liquid anions; effect of introducing ether oxygen into Perfluoroalkylborate on physical and thermal properties, Chem. Commun. 46 (10) (2010) 1730, https://doi.org/ 10.1039/b916759e.
- [13] J. Zhu, L. Bai, B. Chen, W. Fei, Thermodynamical properties of phase change materials based on ionic Liquids, Chem. Eng. J. 147 (1) (2009) 58–62, https://doi.org/10.1016/ j.cej.2008.11.016.
- [14] M. Bendová, Z. Wagner, M.G. Bogdanov, M. Čanji, N. Zdolšek, Heat capacity of 1-Hexadecyl-3-Methylimidazolium based ionic Liquids in solid and liquid phase, J. Mol. Liq. 305 (2020) 112847, https://doi.org/10.1016/j.molliq.2020.112847.
- [15] T. Welton, Room-temperature ionic Liquids. Solvents for synthesis and catalysis, Chem. Rev. 99 (8) (1999) 2071–2084, https://doi.org/10.1021/cr980032t.
- [16] T. Welton, Ionic Liquids: a brief history, Biophys. Rev. 10 (3) (2018) 691–706, https://doi.org/10.1007/s12551-018-0419-2.

- [17] J. Dupont, On the solid, liquid and solution structural Organization of Imidazolium Ionic Liquids, J. Braz. Chem. Soc. 15 (3) (2004) 341–350, https://doi.org/10.1590/ S0103-50532004000300002.
- [18] Ionic Liquids, in: S. Zhang (Ed.), Physicochemical Properties, 1st edElsevier, Amsterdam, The Netherlands; Boston; London, 2009.
- [19] C.P. Fredlake, J.M. Crosthwaite, D.G. Hert, S.N.V.K. Aki, J.F. Brennecke, Thermophysical properties of Imidazolium-based ionic Liquids, J. Chem. Eng. Data 49 (4) (2004) 954–964, https://doi.org/10.1021/je034261a.
- [20] H. Luo, G.A. Baker, S. Dai, Isothermogravimetric determination of the enthalpies of vaporization of 1-Alkyl-3-Methylimidazolium ionic Liquids, J. Phys. Chem. B 112 (33) (2008) 10077–10081, https://doi.org/10.1021/jp805340f.
- [21] P.C. Hillesheim, J.A. Singh, S.M. Mahurin, P.F. Fulvio, Y. Oyola, X. Zhu, D. Jiang, S. Dai, Effect of alkyl and aryl substitutions on 1,2,4-Triazolium-based ionic Liquids for carbon dioxide separation and capture, RSC Adv. 3 (12) (2013) 3981, https://doi.org/ 10.1039/c2ra22646d.
- [22] M.G. Cowan, M. Masuda, W.M. McDanel, Y. Kohno, D.L. Gin, R.D. Noble, Phosphonium-based poly(ionic liquid) membranes: the effect of Cation alkyl chain length on light gas separation properties and ionic conductivity, J. Membr. Sci. 498 (2016) 408–413, https://doi.org/10.1016/j.memsci.2015.10.019.
- [23] J.M. Crosthwaite, M.J. Muldoon, J.K. Dixon, J.L. Anderson, J.F. Brennecke, Phase transition and decomposition temperatures, heat capacities and viscosities of Pyridinium ionic Liquids, J. Chem. Thermodyn. 37 (6) (2005) 559–568, https://doi.org/10.1016/j.jct.2005.03.013.
- [24] A.E. Bradley, C. Hardacre, J.D. Holbrey, S. Johnston, S.E.J. McMath, M. Nieuwenhuyzen, Small-angle X-ray scattering studies of liquid crystalline 1-Alkyl-3-Methylimidazolium salts, Chem. Mater. 14 (2) (2002) 629–635, https://doi.org/10.1021/cm010542v.
- [25] M.A.A. Rocha, C.M.S.S. Neves, M.G. Freire, O. Russina, A. Triolo, J.A.P. Coutinho, L.M.N.B. Santos, F. Alkylimidazolium based ionic Liquids: impact of Cation symmetry on their Nanoscale structural organization. J. Phys, Chem. B 117 (37) (2013) 10889–10897, https://doi.org/10.1021/jp406374a.
- [26] Y. Jeong, J.-S. Ryu, Synthesis of 1,3-Dialkyl-1,2,3-Triazolium ionic Liquids and their applications to the Baylis—Hillman reaction, J. Org. Chem. 75 (12) (2010) 4183–4191, https://doi.org/10.1021/jo100618d.
- [27] L.A. Daily, K.M. Miller, Correlating structure with thermal properties for a series of 1-Alkyl-4-Methyl-1,2,4-Triazolium ionic Liquids, J. Org. Chem. 78 (8) (2013) 4196–4201, https://doi.org/10.1021/jo4003932.
- [28] B. Bittner, R.J. Wrobel, E. Milchert, Physical properties of Pyridinium ionic Liquids, J. Chem. Thermodyn. 55 (2012) 159–165, https://doi.org/10.1016/j.jct.2012.06.018.
- [29] F. Neve, O. Francescangeli, A. Crispini, J. Charmant, A 2 [MX 4] copper(II) Pyridinium salts. From ionic Liquids to layered solids to liquid crystals, Chem. Mater. 13 (6) (2001) 2032–2041, https://doi.org/10.1021/cm000804d.
- [30] P.C. Hillesheim, S.M. Mahurin, P.F. Fulvio, J.S. Yeary, Y. Oyola, D. Jiang, S. Dai, Synthesis and characterization of Thiazolium-based room temperature ionic Liquids for gas separations, Ind. Eng. Chem. Res. 51 (35) (2012) 11530–11537, https://doi.org/10.1021/ie3015632.
- [31] T. Espinosa, J. Sanes, M.-D. Bermúdez, New Alkylether-Thiazolium room-temperature ionic liquid lubricants: surface interactions and Tribological performance, ACS Appl. Mater. Interfaces 8 (28) (2016) 18631–18639, https://doi.org/10.1021/acsami.6b05888.
- [32] Q. Yan, H. Zang, C. Wu, J. Feng, M. Li, M. Zhang, L. Wang, B. Cheng, Synthesis, characterization and catalytic application of novel ionic Liquids based on Thiazolium Cation, J. Mol. Liq. 204 (2015) 156–161, https://doi.org/10.1016/j.molliq.2015.01.016.
- [33] A. Mirjafari, R.A. O'Brien, K.N. West, J.H. Davis, Synthesis of new lipid-inspired ionic Liquids by Thiol-Ene chemistry: profound solvent effect on reaction pathway, Chem. - EurJ. 20 (25) (2014) 7576–7580, https://doi.org/10.1002/chem.201402863.
- [34] A. Mirjafari, Ionic liquid syntheses via click chemistry: expeditious routes toward versatile functional materials, Chem. Commun. 54 (24) (2018) 2944–2961, https://doi.org/10.1039/C8CC00372F.
- [35] Apex3 V2019.1--0, SAINT V8.40A, Bruker AXS Inc, Madison (WI), USA, 2019.
- [36] L. Krause, R. Herbst-Irmer, G.M. Sheldrick, D. Stalke, Comparison of silver and molybdenum microfocus X-ray sources for single-crystal structure determination, J. Appl. Crystallogr. 48 (1) (2015) 3–10, https://doi.org/10.1107/S1600576714022985.
- [37] SHELXTL Suite of Programs, Version 6.14, 2000-2003, Bruker Advanced X-Ray Solutions; Bruker AXS Inc.: Madison (WI), USA.
- [38] G.M. Sheldrick, A short history of SHELX, Acta Crystallogr. A 64 (1) (2008) 112–122, https://doi.org/10.1107/S0108767307043930.
- [39] G.M. Sheldrick, Crystal structure refinement with SHEIXL, Acta Crystallogr. Sect. C Struct. Chem. 71 (1) (2015) 3–8, https://doi.org/10.1107/S2053229614024218.
- [40] C.B. Hübschle, G.M. Sheldrick, B. Dittrich, ShelXle: a Qt graphical user Interface for SHELXL, J. Appl. Crystallogr. 44 (6) (2011) 1281–1284, https://doi.org/10.1107/ S0021889811043202.
- [41] Turner, M. J.; McKinnon, J. J.; Wolff, S. K.; Grimwood, D. J.; Spackman, P. R.; Jayatilaka, D.; Spackman, M. A. CrystalExplorer17; University of Western Australia.
- [42] Dolomanov, O. V.; Bourhis, L. J.; Gildea, R. J.; Howard, J. A. K.; Puschmann, H. OLEX2: A Complete Structure Solution, Refinement and Analysis Program. J. Appl. Crystallogr. 2009, 42 (2), 339–341. doi:https://doi.org/10.1107/S0021889808042726.
- [43] C.F. Macrae, I.J. Bruno, J.A. Chisholm, P.R. Edgington, P. McCabe, E. Pidcock, L. Rodriguez-Monge, R. Taylor, J. van de Streek, P.A. Wood, *Mercury CSD 2.0* new features for the visualization and investigation of crystal structures, J. Appl. Crystallogr. 41 (2) (2008) 466–470, https://doi.org/10.1107/S0021889807067908.
- [44] Y. Cai, Q. Wei, F. Huang, S. Lin, F. Chen, W. Gao, Thermal stability, latent heat and flame retardant properties of the thermal energy storage phase change materials based on paraffin/high density polyethylene composites, Renew. Energy 34 (10) (2009) 2117–2123, https://doi.org/10.1016/j.renene.2009.01.017.

- [45] M.E.V. Valkenburg, R.L. Vaughn, M. Williams, J.S. Wilkes, Thermochemistry of ionic liquid heat-transfer fluids, Thermochim. Acta 425 (1–2) (2005) 181–188, https:// doi.org/10.1016/j.tca.2004.11.013.
- [46] Bonhôte, P.; Dias, A.-P.; Papageorgiou, N.; Kalyanasundaram, K.; Grätzel, M. Hydrophobic, Highly Conductive Ambient-Temperature Molten Salts. 11.
- [47] J.G. Huddleston, A.E. Visser, W.M. Reichert, H.D. Willauer, G.A. Broker, R.D. Rogers, Characterization and comparison of hydrophilic and hydrophobic room temperature ionic Liquids incorporating the Imidazolium Cation, Green Chem. 3 (4) (2001) 156–164, https://doi.org/10.1039/b103275p.
- [48] R. Hayes, G.G. Warr, R. Atkin, Structure and nanostructure in ionic Liquids, Chem. Rev. 115 (13) (2015) 6357–6426, https://doi.org/10.1021/cr500411q.
- [49] T. Steiner, The hydrogen bond in the solid state, Angew. Chem. Int. Ed. 41 (1) (2002) 48–76, https://doi.org/10.1002/1521-3773(20020104)41:1<48::AID-ANIE48>3.0. CO:2-U.
- [50] J.D. Holbrey, W.M. Reichert, M. Nieuwenhuyzen, S. Johnson, K.R. Seddon, R.D. Rogers, Crystal Polymorphism in 1-Butyl-3-Methylimidazolium Halides: Supporting Ionic Liquid Formation by Inhibition of Crystallization, Chem. Commun. (2003) 1636, https://doi.org/10.1039/b304543a No. 14.
- [51] A. Tarahhomi, A. van der Lee, Synthesis and crystal structures of new phosphoric Triamides: study of intermolecular interactions by semi-empirical calculations and Hirshfeld surface analysis. *Monatshefte Für Chem. - Chem*, Mon. 149 (10) (2018) 1759–1776, https://doi.org/10.1007/s00706-018-2186-y.
- [52] J.J. McKinnon, D. Jayatilaka, M.A. Spackman, Towards Quantitative Analysis of Intermolecular Interactions with Hirshfeld Surfaces, Chem. Commun. 37 (2007) 3814, https://doi.org/10.1039/b704980c.
- [53] P.M. Dean, J.M. Pringle, C.M. Forsyth, J.L. Scott, D.R. MacFarlane, Interactions in Bisamide ionic Liquids—insights from a Hirshfeld surface analysis of their crystalline states, New J. Chem. 32 (12) (2008) 2121, https://doi.org/10.1039/b809606f.

- [54] M.A. Spackman, D. Jayatilaka, Hirshfeld surface analysis, CrystEngComm 11 (1) (2009) 19–32, https://doi.org/10.1039/B818330A.
- [55] D.G. Golovanov, K.A. Lyssenko, Ya S. Vygodskii, E.I. Lozinskaya, A.S. Shaplov, M. Yu Antipin, Crystal Structure of 1,3-Dialkyldiazolium Bromides, Russ. Chem. Bull. 55 (11) (2006) 1989–1999, https://doi.org/10.1007/s11172-006-0541-3.
- [56] C. Roth, T. Peppel, K. Fumino, M. Köckerling, R. Ludwig, The importance of hydrogen bonds for the structure of ionic Liquids: single-crystal X-ray diffraction and transmission and attenuated Total reflection spectroscopy in the terahertz region, Angew. Chem. Int. Ed. 49 (52) (2010) 10221–10224, https://doi.org/10.1002/anie. 201004955.
- [57] J.J. McKinnon, M.A. Spackman, A.S. Mitchell, Novel tools for visualizing and exploring intermolecular interactions in molecular crystals, Acta Crystallogr. B 60 (6) (2004) 627–668, https://doi.org/10.1107/S0108768104020300.
- [58] M.C. Ford, M. Saxton, P.S. Ho, Sulfur as an acceptor to bromine in biomolecular halogen bonds, J. Phys. Chem. Lett. 8 (17) (2017) 4246–4252, https://doi.org/10.1021/acs.jpclett.7b01725.
- [59] P. Politzer, J.S. Murray, T. Clark, Halogen bonding and other σ-hole interactions: a perspective, Phys. Chem. Chem. Phys. 15 (27) (2013) 11178, https://doi.org/10. 1039/c3cp00054k.
- [60] J.Y.C. Lim, P.D. Beer, Sigma-hole interactions in anion recognition, Chem 4 (4) (2018) 731–783, https://doi.org/10.1016/j.chempr.2018.02.022.
- [61] K. Dong, S. Zhang, J. Wang, Understanding the hydrogen bonds in ionic Liquids and their roles in properties and reactions, Chem. Commun. 52 (41) (2016) 6744–6764, https://doi.org/10.1039/C5CC10120D.